Soft Matter

RSC Publishing

PAPER

View Article Online
View Journal | View Issue

Cite this: *Soft Matter*, 2013, **9**, 10768

Tailoring the amphiphilicity and self-assembly of thermosensitive polymers: end-capped PEG–PNIPAAM block copolymers†

Zhilong Quan,[ab] Kaizheng Zhu,[b] Kenneth D. Knudsen,[c] Bo Nyström[b] and Reidar Lund*[b]

In this work we report on the synthesis and self-assembly of a thermo-sensitive block copolymer system of *n*-octadecyl-poly(ethylene glycol)-*block*-poly(*N*-isopropylacrylamide), abbreviated as C_{18}-PEG_n-*b*-$PNIPAAM_m$. We present a facile synthetic strategy for obtaining highly tunable thermo-responsive block copolymers starting from commercial PEG-based surfactants (Brij®) or a C_{18} precursor and conjugating with PNIPAAM *via* an Atom Transfer Radical Polymerization (ATRP) protocol. The self-assembly and detailed nanostructure were thoroughly investigated in aqueous solutions using both small-angle X-ray and neutron scattering (SAXS/SANS) combined with turbidity measurements. The results show that the system forms rather well defined classical micellar structures at room temperature that first undergo a collapse, followed by inter-micellar aggregation upon increasing the temperature. For the pure C_{18}-PNIPAAM system, however, rather ill-defined micelles were formed, demonstrating the important role of PEG in regulating the nanostructure and the stability. It is found that the PEG content can be used as a convenient parameter to regulate the thermoresponse, *i.e.*, the onset of collapse and aggregation. A detailed theoretical modeling analysis of the SAXS/SANS data shows that the system forms typical core–shell micellar structures. Interestingly, no evidence of back folding, where PEG allows PNIPAAM to form part of the C_{18} core, can be found upon crossing the lower critical solution temperature (LCST). This might be attributed to the entropic penalty of folding a polymer chain and/or enthalpic incompatibility between the blocks. The results show that by appropriately varying the balance between the hydrophobic and hydrophilic content, *i.e.* the amphiphilicity, tunable thermoresponsive micellar structures can be effectively designed. By means of SAXS/SANS we are able to follow the response on the nanoscale. These results thus give considerable insight into thermo-responsive micellar systems and provide guidelines as to how these systems can be tailor-made and designed. This is expected to be of considerable interest for potential applications such as in nanomedicine where an accurate and tunable thermoresponse is required.

Received 16th July 2013
Accepted 4th September 2013

DOI: 10.1039/c3sm51945g

www.rsc.org/softmatter

Introduction

Stimuli-responsive polymers are intriguing materials that respond directly to small changes in physical or chemical conditions through changes in their conformation and/or solubility. Possible stimuli include temperature, pH, magnetic or electric fields, applied mechanical force, or light.[1–4] These materials play an increasingly important part in a wide range of applications, such as in drug delivery, diagnostics, as well as in biosensors, micro-electromechanical systems, coatings *etc.*[4–6]

Perhaps the most accessible external stimulus is the temperature, which can be used to trigger changes in solubility of thermoresponsive polymers upon either heating or cooling. Among synthetic polymers, poly(*N*-isopropylacrylamide) (PNIPAAM) can be considered to be one of the most extensively investigated thermoresponsive polymers.[2,7–12] PNIPAAM contains a hydrophobic side group that together with the temperature-dependent conformation and hydrogen bonding with water determines the solubility of PNIPAAM in water. PNIPAAM exhibits a lower critical solution temperature (LCST) at an often-reported temperature close to 32 °C for high molecular weight chains in water and a few degrees lower in physiological saline solution.[7–10] However, it has been shown that for narrowly distributed polymer chains, the transition is molecular weight

[a]*College of Materials Science & Engineering, Huaqian University, 361021 Xiamen, P. R. China*

[b]*Department of Chemistry, University of Oslo, P.O.Box 1033, Blindern, N-0315 Oslo, Norway. E-mail: reidar.lund@kjemi.uio.no*

[c]*Department of Physics, Institute for Energy Technology, P. O. Box 40, N-2027 Kjeller, Norway*

† Electronic supplementary information (ESI) available. See DOI: 10.1039/c3sm51945g

and concentration dependent and may vary between 25 and 45 °C.[11–13] Upon heating to above the transition temperature, a coil-to-globule transition occurs that is followed by inter-molecular association if the solution is not too dilute and macroscopic phase separation, often referred to as the cloud point.

In order to control the aggregation behavior of PNIPAAM, the polymer needs to be combined with another block that limits and controls the growth of the association complexes. A straightforward way to achieve this is by covalently adding a water-soluble polymer such as poly(ethylene glycol) (PEG) to PNIPAAM. This yields a double hydrophilic PNIPAAM–PEG block copolymer at room temperature, which again self-assembles into micelles consisting of dehydrated PNIPAAM cores and dissolved PEG in the corona at elevated temperatures.[14,15]

Studies have shown that for larger PNIPAAM blocks even polymeric vesicles can be formed using this strategy.[16] However, to allow the nanostructures to form and also to load the system with, *e.g.*, a hydrophobic drug, the solution needs to be kept at high temperatures. Alternatively, the PNIPAAM might be functionalized with hydrophobic residues such as an octadecyl (C_{18})-group, which promotes self-assembly at lower temperatures.[17] This strategy also includes telechelic PNIPAAM with two C_{18} groups at both ends (C_{18}-PNIPAAM-C_{18}). In this case, depending on the concentration, thermoresponsive micelles as well as hydrogels could be observed.[18–21] Alternatively, PNIPAAM can be functionalized with hydrophobic blocks at both ends, *e.g.*, polystyrene (PS)-based PS-PNIPAAM-PS block copolymers.[22,23] However, these systems form micelles that often have a limited stability range and are prone to phase separation even at moderate temperatures. To obtain suitable nanostructures, the amphiphilicity of the block copolymers needs to be precisely tuned.

One possibility for achieving enhanced control of the self-assembly of PNIPAAM-based systems is to introduce a third polymer block, *i.e.*, triblock terpolymer systems. In a series of studies, Hillmyer, Lodge and co-workers investigated a terpolymer system of poly(ethylene-*alt*-propylene)–PEP–PNIPAAM (PEP–PEG–PNIPAAM).[24–26] These polymers exhibit a stepwise self-assembly mechanism forming "classical" micelles with PEP in the core and hydrophilic PEG/PNIPAAM coronas at low temperatures. Subsequently upon increasing the temperature above the LCST of PNIPAAM, the system undergoes a controlled aggregation into well-defined hydrogels where the strength of the network is given by the inter-chain association between PNIPAAM at the surface of the micelles. This was found to give hydrogels at a much lower concentration than commonly observed for B–A–B-type triblock copolymers.[25] Interestingly, it was suggested that PNIPAAM could not fold back into the PEP core due to the limited miscibility and/or entropic penalty of loop formation. The former incompatibility between blocks represents one of the advantages of A–B–C type terpolymers and is found to result in lower sol–gel concentrations.[25]

In this work, we investigate a system that is designed along similar ideas to triblock terpolymers, but that can be prepared using a more facile synthetic scheme. Instead of using a hydrophobic polymer block, we base our system on PNIPAAM derivatives containing the commercial non-ionic surfactants PEG–octadecylether (Brij®S10, S20 and S100). By utilizing either C_{18}–OH or Brij® as the precursor, PNIPAAM could be grafted at the end of PEG by using atom transfer radical polymerization (ATRP) of the corresponding NIPAAM monomer. Using this method we have successfully prepared *n*-octadecyl-poly(ethylene glycol)-*block*-poly(*N*-isopropylacrylamide), abbreviated as C_{18}-PEG$_n$-*b*-PNIPAAM$_m$, where *n* varies from 0 to 100 and *m* is kept at a near constant value ($m \approx 50$), respectively. By employing turbidity measurements, combined with small-angle X-ray and neutron scattering techniques, we characterize the nanostructure and phase behavior in detail. Contrary to other techniques, SANS/SAXS provides high resolution structural data which, combined with data advanced modeling, provide very detailed *in situ* information on the internal structure and response of the nanostructures. We show that by systematically varying the amphiphilicity of the copolymer system the thermoresponsiveness, as well as the structure and aggregation behavior, can be accurately tuned. As far as we know, this is the first report on this kind of stimuli-sensitive nonionic polymer surfactant system.

Experimental section

Synthesis and materials

Fig. 1 shows the synthetic strategy of the C_{18}-capped-PNIPAAM derivatives *via* an ATRP protocol. The chemical structures of PNIPAAM and its block copolymer derivatives are displayed in Fig. 2 and the selected ^{1}H NMR spectra are given in Fig. 3.

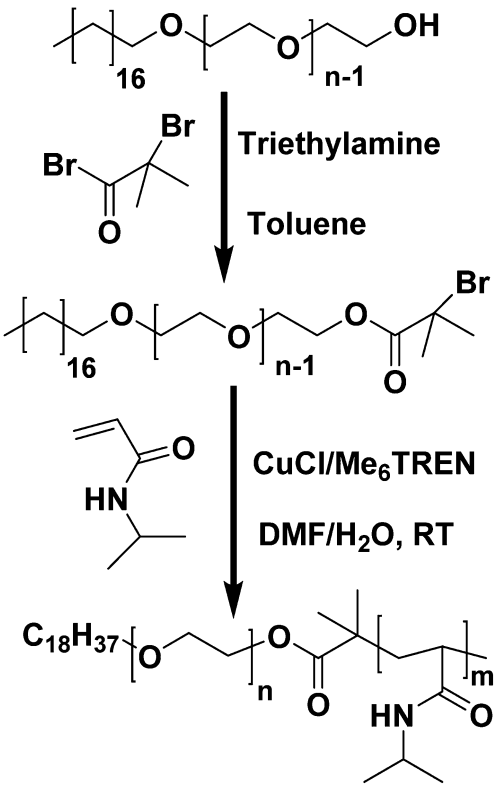

Fig. 1 Synthetic route for the preparation of the C_{18}-capped-PNIPAAM and C_{18}-capped-PEG-*b*-PNIPAAM diblock copolymers ($n = 10$, 20 and 100) *via* the aqueous ATRP procedure.

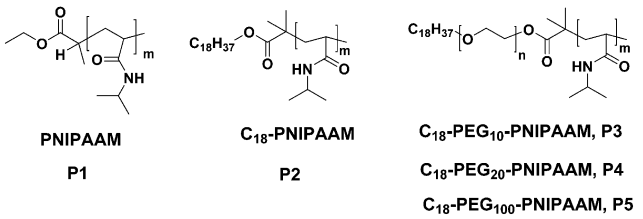

Fig. 2 Chemical structures of the synthesized PNIPAAM and PNIPAAM-derivatives.

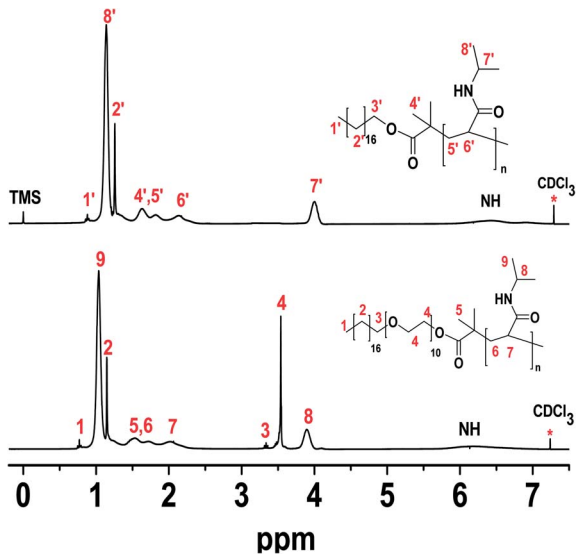

Fig. 3 ^{1}H NMR spectra of the octadecyl-capped PNIPAAM (C_{18}-PNIPAAM) and the selected octadecyl-capped-PEG_{10}-*block*-PNIPAAM diblock copolymer (C_{18}-PEG_{10}-*b*-PNIPAAM) ($CDCl_3$-*d* as the solvent, 300 MHz, 25 °C).

As we can see from Fig. 4, these synthesized PNIPAAM derivatives have a fairly narrow molecular weight distribution. Analyzing the peaks we obtain values for the polydispersity index M_w/M_n between 1.1 and 1.2 (see Table 1). The sharp peaks centered at a retention time of 15–17 min were attributed to the

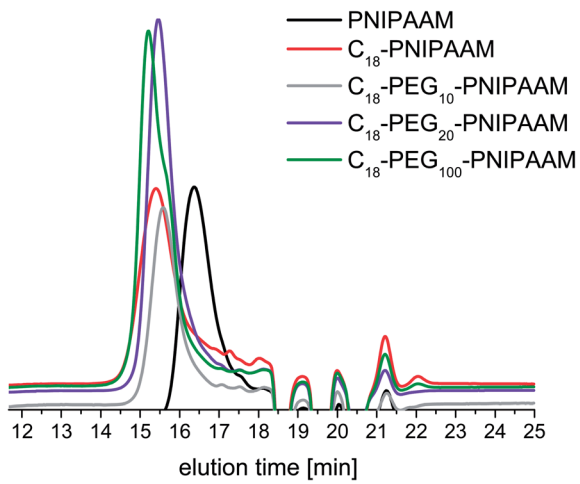

Fig. 4 GPC measurements of the synthesized PNIPAAM derivatives (THF as the eluent, flow rate 1.0 mL min^{-1}, PS as the standard polymer).

Table 1 Chemical composition, number-average molecular weights, and polydispersity indices of the PNIPAAM-derivatives

Polymer	Block No. (*n*/*m*) (NMR)	M_n (NMR)	M_n (GPC)	M_w/M_n (GPC)
P1	0/47	4400	3580	1.15
P2	0/50	6000	9570	1.14
P3	10/57	7230	9310	1.10
P4	20/55	7440	11 470	1.14
P5	100/52	10 620	12 370	1.12

response of the polymers, and the peaks appearing between 18 and 20 min arise from the solvent used in the synthesis, and are commonly observed in GPC.[27,28] A very small shoulder of the C_{18}-PEG-PNIPAAM polymers appearing between 17 and 18 min may be attributed to the small amount of the C_{18}/C_{18}-PEG-macroinitiator left in the sample after purification.

Materials

Octadecanol, poly(ethylene glycol) octadecyl ether (Brij®S10, M_n value of 711, Brij®S20, M_n value of 1150 and Brij®S100, M_n value of 4670) and 2-bromoisobutyl bromide were purchased from Sigma-Aldrich and employed as received. *N*-Isopropylacrylamide (NIPAAM, Acros) was recrystallized from a toluene/*n*-hexane mixture and dried under vacuum before use. Triethylamine (TEA) was dried over anhydrous magnesium sulfate, filtered, distilled under N_2 and stored over 4 Å molecular sieves. Copper(I) chloride from Aldrich was washed with glacial acetic acid, followed by washing with methanol and diethyl ether and then dried under vacuum and kept under a N_2 atmosphere. *N*,*N*,*N*′,*N*″′,*N*″′,*N*″″-(hexamethyl triethylene tetramine) (Me_6TREN) was synthesized according to a procedure described in the literature.[29] The homopolymers of poly(*N*-isopropylacrylamide) ($PNIPAAM_m$, where $m = 47$) used in this study were synthesized *via* an ATRP procedure, which has been described previously.[12] The water used in this study was purified with a Millipore Mill-Q system and the resistivity was *ca.* 18 MΩ cm. The solutions were prepared by dissolving the polymer samples in D_2O, which provides a better contrast and lower incoherent background for SANS. It should be stressed that the same solution was used for all types of measurements (turbidity, SANS, SAXS).

Synthesis of the octadecyl initiator (C_{18}-Br) and octadecyl-capped poly(ethylene glycol) initiator (C_{18}-PEG_n-Br, $n = 10$, 20 and 100). The octadecyl-capped initiator (C_{18}-Br) and octadecyl-capped-PEG macroinitiator (C_{18}-PEG-Br) were prepared by reacting octadecanol (C_{18}-OH) or poly(ethylene glycol) octadecylether (C_{18}-PEG-OH) with 2-bromoisobutyl bromide in the presence of triethylamine as outlined in Fig. 1.[30,31] The ^{1}H-NMR spectra indicated that the degree of esterification was at least 99% (Fig. S1, S2, S4 and S6, ESI†).

The repeating units of ethylene glycol (EG) in the PEG polymers were recalculated according to the ^{1}H NMR spectra (Fig. S4 and S6, ESI†) of the fully esterified products, based on a simple formula: $n = (3I_a/2I_b)$, where I_a is the corresponding integral area of the methenyl group of EG (–O–CH_2CH_2–) at 3.7 ppm and

I_b is the integral area of the end-capped methyl group (–C(CH_3)$_2$Br, 6H) at 1.9 ppm. The number of repeating units of EG were estimated to be 10 for Brij®S10, 20 for Brij®S20 and 100 for Brij®S100, and they are designated as C_{18}-PEG_{10}, C_{18}-PEG_{20} and C_{18}-PEG_{100}, respectively.[31,32]

Synthesis of the C_{18}-capped PNIPAAM and C_{18}-PEG-*b*-PNIPAAM. The C_{18}-capped PNIPAAM and the C_{18}-capped-PEG_n-*b*-PNIPAAM diblock copolymers (n = 10, 20 and 100) were prepared *via* a simple atom transfer radical polymerization (ATRP) procedure (Fig. 1). Briefly, the polymerization was performed in a solvent mixture of water/DMF (40/60, v/v) at 25 °C, and the initiator/catalyst system in the mixture contained the C_{18}-initiator (C_{18}-MI) or PEG-functional macroinitiator (C_{18}-PEG_n-MI), CuCl and Me_6TREN (with a molar feed ratio ([NIPAAM] = 1 M) [NIPAAM]/[C_{18}-PEG_n-MI]/[CuCl]/[Me_6TREN] = 60/1/1/1). The preparation and purification procedures of the polymers were conducted under similar conditions as described in detail previously.[12,31–34]

The chemical structure and composition of the PNIPAAM derivatives were also ascertained by their ^{1}H NMR spectra (Fig. 3). The number-average molecular weight and the unit numbers of n and m in C_{18}-PEG_n-*b*-P(NIPAAM)$_m$ were assessed by comparing the integral area of the methyne proton (8 in Fig. 3) of PNIPAAM (δ = 3.85 ppm, –CH(CH_3)$_2$, I_a) and the methenyl proton peak (4) of EG (δ = 3.70 ppm, –OCH_2CH_2O–, I_b) based on a simple equation: $n_{(NIPAAM)} = m(4(I_a/I_b))$. The repeating units of NIPAAM of C_{18}-PNIPAAM were determined by comparing the integral area of the end methyl (1′, 1 in Fig. 3) group (δ = 0.8 ppm, CH_3(CH_2)$_{16}$CH_2O–, I_c) of the long C_{18}-group and the methyne proton (7′, 8 in Fig. 3 and 8 in Fig. S7, ESI†) of PNIPAAM (δ = 3.85 ppm, –CH(CH_3)$_2$, $I_{a'}$) n based on a simple equation: $n'_{(NIPAAM)} = 3(I_{a'}/I_c)$. The calculated results of the repeating units of NIPAAM of C_{18}-PNIPAAM (n' = 50) and C_{18}-PEG-*b*-PNIPAAM diblock copolymers (n = 57, 55 and 52 for C_{18}-PEG_{10}, C_{18}-PEG_{20} and C_{18}-PEG_{100}, respectively) are displayed in Table 1.

Gel permeation chromatography (GPC) measurement

The molecular weights and polydispersity indices (M_w/M_n) of the synthesized PNIPAAM derivatives were determined by using a Perkin-Elmer 200 GPC instrument, operating at 40 °C, which comprised of two PL gel 5 μm Mixed D columns (300 × 7.5 mm) and a differential refractive index detector. Polystyrene standard samples were used for the calibration procedure, and the measurements were carried out by using tetrahydrofuran (THF) as the eluent with an elution rate of 1.0 mL min^{-1}.

Turbidity

The temperature dependences of the turbidity of the copolymer solutions were monitored at a heating rate of 0.2 °C min^{-1} by employing an NK60-CPA cloud point analyzer from Phase Technology, Richmond, BC, Canada. A detailed description of the apparatus and the determination of turbidities have been given elsewhere.[35] This apparatus makes use of a scanning diffusive technique to characterize phase changes of the samples with high sensitivity and accuracy. The light beam from a laser source, operating at 654 nm, was focused on the solution that was placed on a specially designed glass plate that is coated with a thin metallic layer of very high reflectivity. Directly above the applied sample, an optical arrangement with a light scattering detector continuously monitors the scattered intensity signal (S) from the measured solutions as it is subjected to prescribed temperature alterations. The turbidity is defined as $\tau = (-1/d)\ln(I/I_0)$, where I_0 and I are the transmitted beams of the sample and solvent, respectively, and d is the light path.

Small-angle X-ray scattering experiments (SAXS)

The synchrotron SAXS experiments were performed on the bioSAXS high-throughput P12 EMBL beamline located on the PETRA III storage ring at DESY, Hamburg. The instrument is equipped with a Pilatus 2M detector and the measurements were carried out in a Q-range of 0.0076–0.46 Å^{-1}. The data acquisition was executed by injecting a 10 μL amount of sample into quartz capillaries (2 mm) using 20 successive frames with 50 s exposures that were later added to improve the statistics. No sign of beam radiation damage was observed under these conditions. The data were averaged after normalization to the intensity of the transmitted beam and calibrated on an absolute scale using Millipore water as a primary calibrating standard.

Small-angle neutron scattering experiments (SANS)

Small-angle neutron scattering (SANS) experiments were carried out with the SANS installation at the JEEP II reactor, Kjeller, Norway. The wavelength used was 5.1 and 10.2 Å, with a resolution ($\Delta\lambda/\lambda$) of 10%. The Q range employed in the experiments was 0.008–0.25 Å^{-1}, where $Q = (4\pi/\lambda)\sin(\theta)$ and 2θ is the scattering angle. The polymer solutions were filled in 2 mm Hellma quartz cuvettes (with stoppers), which were placed on a copper base for good thermal contact and mounted in the sample chamber. Standard reductions of the scattering data, including transmission corrections, were conducted by incorporating data collected from an empty cell, beam without the cell, and blocked-beam background. The data were finally transformed to an absolute scale (coherent differential scattering cross-section ($d\Sigma/d\Omega$)) by calculating the normalized scattered intensity from direct beam measurements.

Theoretical modeling of scattering data

The model fitting of the scattering data was made on an absolute scale taking into account the molecular parameters of the system (see Synthesis and materials). The scattering length densities for both X-rays and neutrons were calculated based on the densities reported in the literature for PEG and C_{18}.[35] Based on these values we obtain for C_{18}: $\rho = 7.54 \times 10^{10}$ cm^{-2} and $\rho = -0.34 \times 10^{10}$ cm^{-2} for X-rays and neutrons, respectively. For PEG we used $\rho = 11.1 \times 10^{10}$ cm^{-2} (SAXS) and $\rho = 0.64 \times 10^{10}$ cm^{-2} (SANS). For PNIPAAM the density was measured to be 1.135 g mL^{-1} at 20 °C and consequently: $\rho = 0.85 \times 10^{10}$ cm^{-2} and $\rho = 10.6 \times 10^{10}$ cm^{-2} for SANS and SAXS, respectively.

In the data modeling we assumed that micelles formed by diblock copolymers can be described by a core–shell form

factor, while for linear PNIPAAM homopolymers we used a general form factor for excluded volume polymer chains.[36] Based on earlier work,[38–41] the core–shell model can be written in the following form assuming monodisperse star-like spherical entities:

$$I(Q) = S(Q)\frac{\phi}{PV_{BCP}}\Big(\Delta\rho_{cp}{}^2P^2V_{cp}{}^2A(Q)_C{}^2 + \Delta\rho_{sp}{}^2P(P-F(0)_{blob})V_{sp}{}^2A(Q)_{sh}{}^2 + 2\Delta\rho_{cp}\Delta\rho_{sp}P^2V_{PEO}V_{cp}A(Q)_cA(Q)_{sh} + V_{sp}{}^2\Delta\rho_{sp}{}^2F(Q)_{blob}(Q)\Big) \quad (1)$$

where P is the aggregation number (average number of chains per micelle), ϕ is the volume fraction, and $V_{BCP} = V_{cp} + V_{sp}$ is the total molar volume of the block copolymer. V_{cp} is the volume of C_{18} and V_{sp} is given by: $V_{sp} = V_{PNIPAAM} + V_{PEG}$. $\Delta\rho_i = \rho_i - \rho_0$ is the contrast determined by the scattering length density difference between the polymer block (shell-forming polymer (i = sp) or core-forming polymer (i = cp)) and the solvent (i = 0). F(Q) is the form factor of a single polymer chain.[37]

It should be mentioned that optionally PNIPAAM can be considered to be in the core, which is easily included in the model by letting $V_{cp} = V_{PNIPAAM} + V_{C18}$ and $V_{sp} = V_{PEG}$. The scattering amplitude of the shell, $A(Q)_{sh}$, was calculated using:

$$A(Q)_{sh} = \exp(-Q^2\sigma_{int}{}^2/2)\frac{1}{C}\int_{Rc}^{\infty}4\pi r^2n(r)\frac{\sin(Qr)}{Qr}dr \quad (2)$$

Here σ_{int} is the width of the core–corona interface and R_c is the radius of the core. $n(r)$ is a density profile for the corona for which we chose a flexible power-law profile multiplied with a cut-off function:

$$n(r) = \frac{r^{-x}}{1 + \exp\Big((r-R_m)/\sigma_mR_m\Big)} \quad (3)$$

where R_m and σ_m are the outer cut-off radius and smearing of the density profile, respectively, and x is a scaling exponent that takes a value of x = 4/3 for star-like structures.[45,46] For the micellar core the scattering amplitude is:

$$A(Q)_c = \exp(-Q^2\sigma_{int}{}^2/2)\frac{3\Big(\sin(QR_c) - QR_c\cos(QR_c)\Big)}{(QR_c)^3} \quad (4)$$

To take into account finite inter-micellar interference effects, a structure factor was included. For simplicity we used the Percus–Yevick structure factor valid for hard spheres with an effective volume fraction η_{HS} and radius R_{HS}.[42] In the case where attractive rather than repulsive interactions were observed, either the Baxter model for hard spheres with short-range attractive interactions[43] or the "Teixeira structure factor"[44] describing formation of particles arranged in "fractal clusters" of cut-off length ξ and fractal dimension d_f was used. The Teixeira model can be written as

$$S(Q)_{fractal} = 1 + \frac{1}{(QR_m)_f^d}\frac{d_f\Gamma(d_f-1)}{\Big[1+1/(Q^2\xi^2)\Big]^{(d_f-1)/2}} \times \sin\Big[(d_f-1)\tan^{-1}(Q\xi)\Big] \quad (5)$$

where $\Gamma(x)$ is the gamma function.

In addition a constant, B, was added to take into account a Q-independent background in the SANS data. Finally, the theoretical fit functions were averaged over the experimental distribution in Q using a resolution function described previously.[47]

Results and discussion

Structural properties at room temperature

To investigate the nanostructure in solution, SAXS measurements were performed at the P12 bioSAXS beamline at EMBL/DESY. The scattering curves showing the normalized absolute intensity (the macroscopic scattering cross-section $d\Sigma/d\Omega$), plotted as a function of the module of the scattering vector, Q ($Q = 4\pi\sin(\theta)/\lambda$, where 2θ is the scattering angle and λ is the wavelength), are shown in Fig. 5 for all considered polymers including the linear PNIPAAM.

As expected, the hydrophobic modification (C_{18} end-capping) of PNIPAAM leads to micellar-like aggregate structures. This is particularly clear when comparing C_{18}-PNIPAAM with linear PNIPAAM in Fig. 5. While PNIPAAM displays a typical scattering pattern of a dissolved polymer chain, the scattered intensity of C_{18}-PNIPAAM is significantly higher with a strong decay at intermediate Q. Similarly, C_{18}-PEG_{20}-PNIPAAM and C_{18}-PEG_{100}-PNIPAAM form typical spherical micelle-like structures. Interestingly, for C_{18}-PEG_{100}-PNIPAAM a slight depletion of the intensity at low-Q is observed, indicating repulsive inter-micellar interactions. This is different from C_{18}-PNIPAAM where the intensity continuously increases at low Q and thus shows no evidence of repulsive interactions. Hence, introducing PEG into the shell induces an additional repulsion that stabilizes the micelles.

To gain further insight into the structure, the data were analyzed with the detailed fitting models outlined above. For PNIPAAM, the data can be readily described using a simple

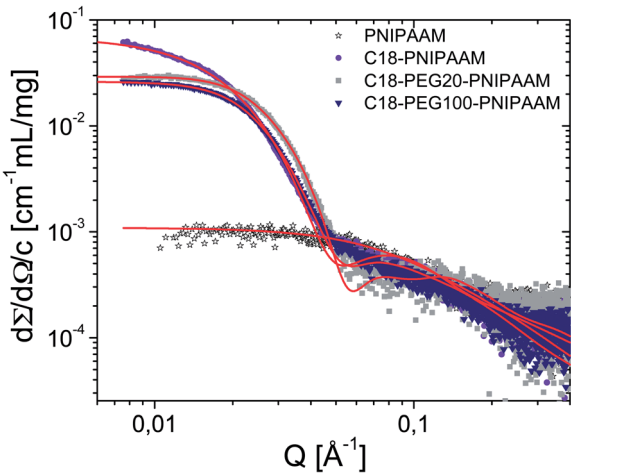

Fig. 5 Small-angle X-ray scattering data showing the scattered intensity as a function of Q for 1% PNIPAAM, C_{18}-PNIPAAM, C_{18}-PEG_{20}-PNIPAAM and C_{18}-PEG_{100}-PNIPAAM in D_2O at room temperature. Solid lines display fits for a spherical core–shell model or linear polymer chains.

form factor model for excluded volume chains[37] giving a radius of gyration, $R_g = 19 \pm 2$ Å. The slope of the scattered curve in Fig. 5 at high-Q was compatible with a fractal dimension of about 1.7, valid for polymer chains exhibiting excluded volume monomer–monomer interactions.

For C_{18}-PNIPAAM the data were fitted using a spherical core–shell fit model indicating an aggregation number of about 66 and an overall micellar radius of about $R_m = 75$ Å. However, as seen in Fig. 5 the fit model does not provide a very good description of the data, in particular not at intermediate Q where the experimental data are more "smeared ", *i.e.* lacking pronounced oscillations. This can be attributed to a distribution of micellar sizes, *i.e.* polydispersity. Since the solution was observed to be slightly turbid already at room temperature, this can be a sign of incipient phase separation. Consequently, we did not attempt to refine the scattering model, which would require an assumption of the distribution function that is problematic under these conditions. We will return to the question of phase stability below.

For the diblock copolymers containing PEG, however, the scattering data can be rather well fitted with the core–shell model outlined above. A very good description can be obtained assuming a simple classical micellar structure, where C_{18} constitutes the core and PEG/PNIPAAM the corona. The fits gave $P = 32$ and 19, for C_{18}-PEG_{20}-PNIPAAM and C_{18}-PEG_{100}-PNIPAAM, respectively, while the cut-off radius of the corona was found to be 113 Å and 94 Å, respectively. Hence, the structure of the micelles follows a rather classical behavior where the aggregation tendency decreases upon an increase in the corona chain length due to an increased spontaneous curvature. From the theory of Daoud and Cotton[45] for star-like polymers, later adapted by Halperin[46] for star-like block copolymer micelles, one would expect a very weak dependence of P on the corona molecular weight, $P \sim M_B^{4/5} \ln[R_m/R_c - 1]^{-6/5}$ where M_B is the molecular weight of the core-forming block. By inserting the numbers, this would predict a reduction of P with a factor of $P(PEG_{20})/P(PEG_{100}) \sim 1.33$, *i.e.* from $P = 32$ to $P = 24$ for C_{18}-PEG_{100}-PNIPAAM. This is fairly close to what is observed experimentally, $P = 19$. For the micellar radius, we would expect the radius to be mainly determined by $R_m \sim P^{1/5} M_A^{3/5}$, where M_A is the molecular weight of the corona-forming chains. Consistent with the assumption of the fits, we assume that the corona chains can be treated as one entity and we calculate $R_m(PEG_{100})/R_m(PEG_{20}) = 1.12$, that is not far from the value observed experimentally: ≈1.2.

As previously mentioned, the slight depression of the intensity at low Q for C_{18}-PEG_{20}-PNIPAAM and C_{18}-PEG_{100}-PNIPAAM indicates repulsive interactions. From the data fits where a Percus–Yevick structure factor was included, this translates into a hard-core radius of 106 and 100 Å with an effective volume fraction of about 0.05 and 0.025 for the copolymers with PEG_{100} and PEG_{20}, respectively. The predominantly repulsive inter-micellar interaction potential was also confirmed in a preliminary study of C_{18}-PEG_{20}-PNIPAAM, where an increased depression of the forward scattering was observed at higher concentrations. However, as the LCST of PNIPAAM is expected to change with concentration, the aggregation behavior of the block copolymer might change in a non-trivial way. A full understanding of this point would require rather extensive systematic studies of the self-assembly, inter-micellar potential and phase behavior at elevated concentrations. These studies will be continued and addressed in a future publication. Nevertheless, the repulsive interactions provide additional evidence that the micelles behave rather classically at room temperature where the hydrophobic C_{18} forms the core and PEG/PNIPAAM constitutes the shell, and the entity exhibits significant excluded volume interactions. To gain further insight into the structure, a selected sample was also directly compared using both SAXS and SANS.

Comparison of SAXS and SANS results: simultaneous model fits

To establish further confidence in the structure, a sample containing 1% C_{18}-PEG100-PNIPAAM in D_2O was investigated at room temperature using both SAXS and SANS. The results are given in Fig. 6.

Fig. 6 clearly demonstrates the significantly different scattering contrast for X-rays and neutrons, where the SAXS data are about one order of magnitude lower in intensity than SANS. Nevertheless, the data can be described simultaneously in a joint fit using the same spherical core–shell model without any further parameters. The results of the fit analysis are shown in Fig. 6. It is clear that the fitted lines describe the data relatively well although some slight deviations are observed. Nevertheless, the results can be seen to be consistent for both techniques, demonstrating the accuracy of the modeling and giving additional confidence in the suggested structure. The data could be described with similar fit parameters although a slightly smaller R_m of 104 Å and larger $\sigma_m = 0.16$ were observed. In the remainder of this work we will focus on the SANS results, which for practical reasons are more suitable for investigation of the structure at elevated temperatures because the samples

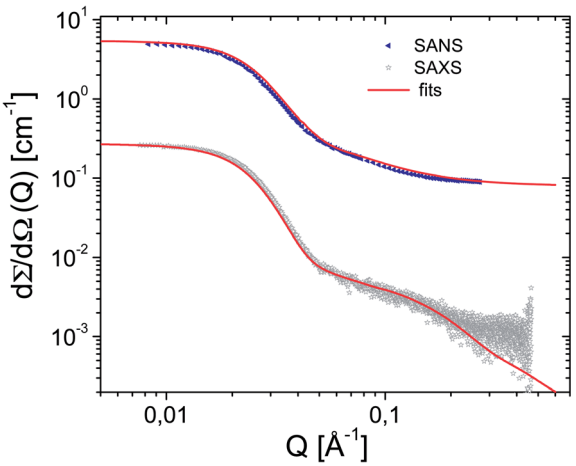

Fig. 6 Comparison of SAXS and SANS data for 1% C_{18}-PEG_{100}-PNIPAAM in D_2O. Solid lines represent a simultaneous fit at an absolute scale using the same spherical core–shell scattering model. Note that no additional shift factors have been introduced. The only additional parameter is a flat instrumental background present for the SANS data.

can be equilibrated for longer times (typically hours) with the set-up we have for SANS. The self-assembly performance and structure at elevated temperatures are addressed in the next section.

Temperature dependence: turbidity

Before focusing on the local structure, the samples were characterized on a more macroscopic scale using turbidimetry, where the transmission of light was monitored as a function of temperature. The turbidity is plotted as a function of temperature for the different block copolymers and PNIPAAM solutions of 1% in Fig. 7. As a comparison also a linear PNIPAAM is included. As expected,[9,11] PNIPAAM exhibits a sharp transition to a turbid solution at a temperature of about 34–35 °C. Defining the cloud point, T_{cp}, as the temperature where the turbidity first starts to increase, we obtain a $T_{cp} = 34$ °C for this concentration and molecular weight. It should be recalled that the cloud point of the pure PNIPAAM depends on both molecular weight and concentration.[11–13] In this work both variables were fixed.

For the end-capped C_{18}-PNIPAAM we observe intrinsic higher values of turbidity even at lower temperatures. This is accompanied by a shift in the cloud point towards lower temperatures to *ca.* 32 °C. However, it should be mentioned that upon storing the sample for a longer time at room temperature, increased visual turbidity was noticed. The tendency for aggregation also increased significantly with increasing polymer concentration. This suggests that the polymer may grow into rather large species following a more "open aggregation behaviour" approaching a macroscopic phase separation. The addition of a C_{18}-group yields an increased hydrophobicity to the polymer, sufficient to destabilize the system. Interestingly, the added hydrophobic character does not seem to lead to well-controlled micelle formation, which might be due to some disruption of hydrogen bonds with water.

For the C_{18}-PEG_{20}-PNIPAAM and C_{18}-PEG_{100}-PNIPAAM polymers, however, a shift is observed towards higher cloud point temperatures located at approximately 38 and 41 °C, respectively. This can be attributed to the increased solubility provided by PEG and probably a tendency to form more stable micelles. At elevated temperatures, the system undergoes macroscopic phase separation. Below we will investigate the detailed structure by SANS.

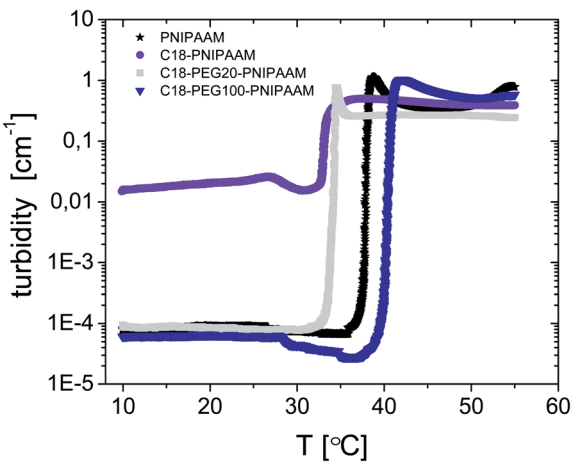

Fig. 7 Turbidity curves. The measured turbidity plotted as a function of temperature for the indicated polymers.

Temperature dependence: mesoscopic structure evolution by SANS

In the following we will focus on the temperature dependence of the detailed structure of micelles formed by C_{18}-PEG_{20}-PNIPAAM/C_{18}-PEG_{100}-PNIPAAM. In the case of PNIPAAM and C_{18}-PNIPAAM, a trivial macroscopic phase separation was observed at augmented temperatures and this phenomenon was not further investigated. Fig. 8 displays the SANS data, including fits, for C_{18}-PEG_{20}-PNIPAAM (a) and C_{18}-PEG_{100}-PNIPAAM (b).

Let us first consider the copolymer with the lowest PEG content, C_{18}-PEG_{20}-PNIPAAM, where rather small structural changes with temperature are observed up to about 40 °C. However, a close inspection of the data at low Q reveals a significant upturn of the intensity. Such a behavior suggests the start of cluster formation, *i.e.*, an incipient aggregation.

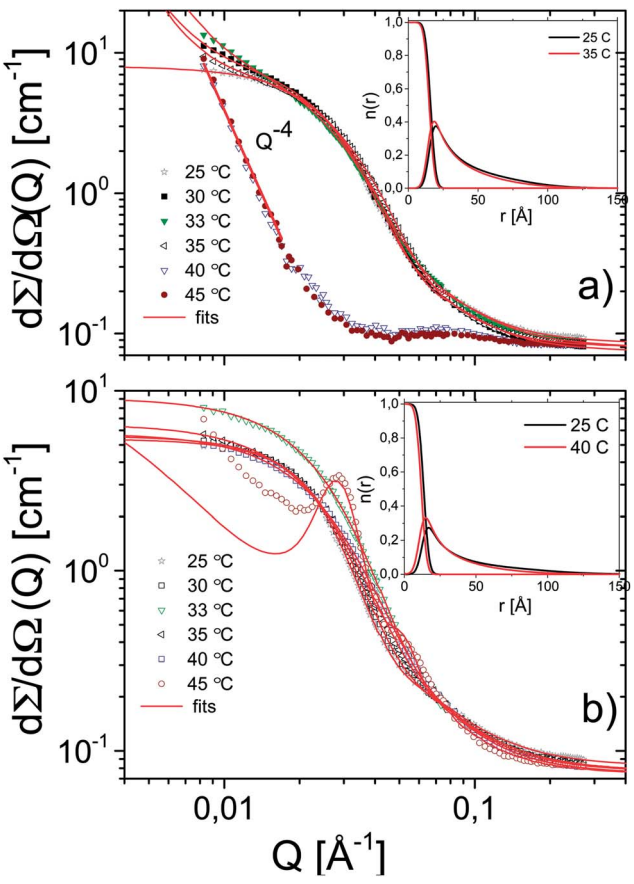

Fig. 8 Small-angle neutron scattering data for (a) C_{18}-PEG_{20}-PNIPAAM and (b) C_{18}-PEG_{100}-PNIPAAM at different temperatures. The polymer concentration was held fixed to 1% in all cases. The solid lines display fits to the core–shell scattering models described in the text. The inset shows the extracted density profile for two selected temperatures.

Table 2 Structural parameters deduced from the model for C_{18}-PEG_{20}-PNIPAAM in D_2O at various temperatures. P is the aggregation number, R_m the overall micellar radius, σ_m outer roughness/profile smearing (in fraction of R_m), R_c the core radius, R_{HS} the hard core radius, SQ the type of structure factor (see below), ξ the cluster size, d_f the fractal dimension and B the instrumental background[a]

T	P	R_m/Å	σ_m	R_c/Å	η_{HS}	R_{HS}/Å	SQ	ξ/nm	d_f	B cm^{-1}
25	32 ± 2	94	0.17	16	0.026	101	PY	—	—	0.08
30	30 ± 3	90	0.16	16	—	—	Fractal	1000 ± 30%	3	0.07
33	28 ± 2	82	0.25	15	—	—	Fractal	1000 ± 30%	3	0.08
35	26 ± 2	77	0.22	15	—	—	Fractal	1000 ± 30%	3	0.08

[a] SQ – structure factor model, PY – Percus–Yevick hard sphere, fractal – fractal cluster (Teixeira) model.

Further increase in temperature to 40 °C leads to drastic changes in the shape of the scattering curves with a very low intensity at high Q and a strong Q^{-4} upturn at low Q. Such an appearance is characteristic of large irregular aggregates that undergo sedimentation and this behavior agrees with the turbidity data that show a strongly reduced transmittance of light at these temperatures. For temperatures below 40 °C, the data can be described using a simple core–shell model including a structure factor for irregular fractal clusters. Since only the "wing" of the cluster scattering at low Q can be observed, the fit analysis only reveals an apparent aggregate size, ξ, of about 1000 nm with a fractal dimension close to 3, *i.e.*, reminiscent of a compact cluster. The range of values of ξ for which good fits could be obtained was found to be typically ±30%. The size of the individual micelles is found to slightly decrease with rising temperature from *ca.* 94 to 77 Å in the temperature interval of 25 to 35 °C, and this trend is accompanied by a weaker reduction of the aggregation number from 32 to 26. The important micellar structural parameters are given in Table 2.

The corresponding temperature dependence of the scattered intensity from C_{18}-PEG_{100}-PNIPAAM is given in Fig. 8(b) and the structural parameters deduced from the fit analysis are given in Table 3. In this case a pronounced temperature dependence can be observed. Interestingly, the overall scattered intensity initially increases from 25 to 33 °C, indicating an increase in the aggregation number. In addition, we observe a concomitant shift of the scattered intensity towards a higher Q, which suggests a reduction in the micellar dimension. Upon further increase in temperature a decrease in both aggregation number and micellar size can be detected.

To better visualize the structural changes, the radial density profiles, $n(r)$, deduced from the fits, are compared and depicted for two temperatures in the insets of Fig. 8. As seen for C_{18}-PEG_{20}-PNIPAAM in Fig. 8(a), the density distribution for the corona shows a small shift towards lower r-values with increasing temperature, *i.e.*, we observe a compaction towards the core. A similar tendency is observed for the C_{18}-PEG_{100}-PNIPAAM sample, where an increasing amount of the corona chains is located closer to the core. Thus, since PEG is not expected to change its solubility drastically at this temperature, it is evident that the corona of PNIPAAM undergoes a partial collapse upon a temperature rise. However, the scattering data do not indicate that PNIPAAM folds back and constitutes a part of the core. This scenario was evaluated from the data modeling by assuming a dry PNIPAAM/C_{18} core with folded PEG chains in the corona. Such a scenario is not compatible with the experimental data, as it would lead to significant excess scattered intensity at high Q. This can be attributed to the entropic penalty of back folding and/or incompatibility of the blocks. However, it is interesting to point out that the density profiles in the insets of Fig. 8 do indicate a compression of the density profile. But, possibly because of the incompatibility between the blocks and the entropic penalty of back folding, no intermixing in the core is observed even above the LCST.

It is clear that both C_{18}-PEG_{20}-PNIPAAM and C_{18}-PEG_{100}-PNIPAAM samples follow a two-step self-assembly process, where the system first undergoes micellization, which gradually results in collapse of the complexes and aggregate formation upon increasing the temperature analogous to what has been proposed for triblock terpolymers.[24–26] The temperature dependence of the micellar structure is analyzed in more detail below.

The extracted aggregation number and the effective micellar radius defined as $R_{tot} = R_m \cdot (1 + \sigma_m)$ are depicted as a function of temperature in Fig. 9.

For typical charged surfactant micelles, the aggregation number is expected to decrease upon increasing the temperature[48], whereas for ethylene oxide (EO) based non-ionic micelles, temperature-induced growth is expected.[49] Similarly P is observed to increase[50] in systems of C_{18}-PEO (Brij®), which corresponds to the precursor polymer. This behavior is ascribed to the inverse solubility appearance for PEG, which is reflected in a LCST around 100 °C.[51]

Table 3 Structural parameters for C_{18}-PEG100-PNIPAAM in D_2O at various temperatures. P is the aggregation number, R_m the overall micellar radius, σ_m the outer roughness (in fraction of R_m), R_c the core radius, R_{HS} the hard core radius, SQ the type of structure factor (see below), ξ the cluster size, d_f the fractal dimension and B the instrumental background. Tau controls the depth of the short range attractive interactions in the Baxter model

T/°C	P	R_m/Å	σ_m	η_{HS}	R_{HS}/Å	R_c/Å	Tau	SQ[a]	B cm^{-1}
25	19 ± 1	114 ± 3	0.14	0.05	107	13	—	PY	0.08
30	18 ± 2	103 ± 2	0.18	0.04	106	13	—	PY	0.08
33	21 ± 2	89 ± 2	0.20	—	—	14	—	—	0.08
35	14 ± 1	84 ± 2	0.26	—	—	12	—	—	0.08
40	13 ± 1	75 ± 2	0.29	—	—	12	—	PY	0.07
45	13 ± 2	75 ± 2	0.25	0.3[b]	132	19	0.056	SHS	0.08

[a] SQ – structure factor model: SHS – sticky hard sphere (Baxter model), PY – Percus–Yevick hard sphere, fractal – fractal cluster (Teixeira) model. [b] Apparent effective volume fraction.

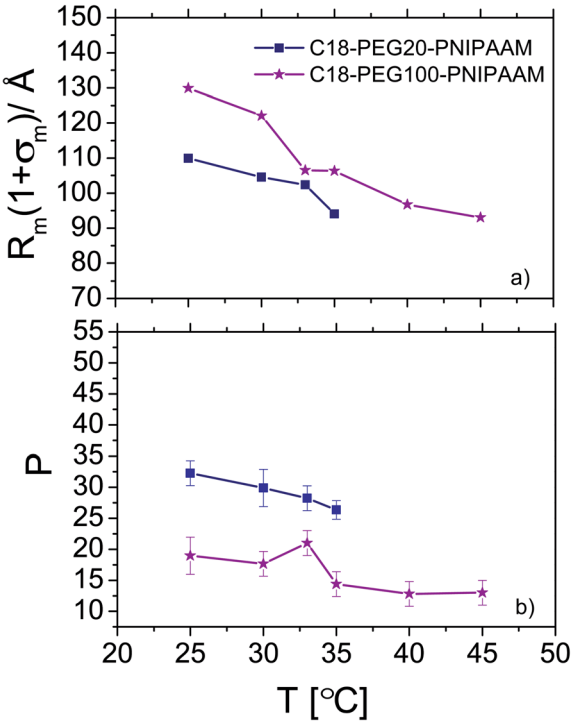

Fig. 9 Temperature dependence of (a) the effective micellar radius and (b) the aggregation number as deduced from the fit analysis of the scattering data.

Comparing the data, C_{18}-PEG_{20}-PNIPAAM exhibits a monotonous decrease in both the aggregation number and effective micellar radius as the temperature increases. As already mentioned, the system undergoes a complete phase separation at high temperatures. C_{18}-PEG_{100}-PNIPAAM seems to undergo a slight initial increase in P, followed by a reduction. The radius, however, decreases linearly up to 40–45 °C.

The system generally exhibits an opposite trend compared to Brij that must be attributed to the influence of PNIPAAM. In the case of C_{18}-PEG_{100}-PNIPAAM, which has the highest content of PEG, the micellization seems to follow a more intermediate appearance. To rationalize this, several (competing) effects must be considered. First, the reduced excluded volume interactions with increasing temperature for both PEG and PNIPAAM must be considered. This leads to shrinkage of the polymers, and in the case of PNIPAAM, even to collapse upon heating. This results in reduced inter-chain repulsion in the corona that gives rise to an increased preferential aggregation number. However, temperature induced collapse leads to, as revealed by the density profiles in Fig. 8, an increased accumulation of chains closer to the core. This may result in a higher spontaneous curvature of the micelles, and thus a reduction in the aggregation number. In addition, hydrogen bonds, present below LCST, are likely to change the interactions within the corona and destabilize the micelles. Upon crossing the LCST, inter-micellar aggregation occurs where the micelles mainly maintain their integrity. This is particularly clear for C_{18}-PEG_{100}-PNIPAAM at 45 °C in Fig. 8. Here we observe a well-defined correlation peak suggesting a preferred inter-micellar distance, as well as an upturn at low Q which would indicate attractive interactions. Comparing with the fits, the scattering pattern can be described using a structure factor for hard spheres with short-range attractions (Baxter model). This model takes into account attractive interactions (responsible for the upturn at low Q) with a preferable inter-micellar distance that is not observed for C_{18}-PEG_{20}-PNIPAAM, which rather exhibited a direct formation of unstructured (random) fractal clusters at higher temperatures. It is tempting to interpret the difference as residual repulsive interactions due to the higher fraction of PEG. It should be mentioned however, that the fitting approach using the Baxter model yields an unreasonably high effective volume fraction of about 0.3 indicating a drastic local densification of the micelles. This may be an artifact due to a phase separation that can be arrested within the SANS cells upon precipitation. Nevertheless, it is clear that both polymers undergo a transition from repulsive to attractive inter-micellar interactions at higher temperatures. This attractive potential eventually leads to aggregation and phase separation. The strength of the interactions and stability range of the micelles as well as the onset of the transition can be accurately tuned with the PEG content.

Finally, we comment on the temperature dependent interaction between micelles observed through the structure factor model fits. For the C_{18}-PEG_{20}-PNIPAAM sample we observe temperature-induced attractive interactions that lead to some aggregation in terms of fractal clusters. For the polymer with the longer PEG, C_{18}-PEG_{100}-PNIPAAM, a more gradual change from repulsive interactions at ambient temperatures to no, or even attractive, interactions at higher T occurs. This is reflected in a decreasing effective volume fraction from about 0.05 to 0.03 followed by a vanishing inter-micellar repulsion ($\eta_{HS} = 0$).

Conclusions

In this work, we have demonstrated an efficient synthetic strategy to generate a family of PNIPAAM-based thermo-sensitive block copolymers. By systematically changing the amphiphilicity of the system, we have shown that control of the self-assembly and thermo-response can be obtained. The results show that the self-assembly of copolymers consisting of PNIPAAM can be tuned by a balance of a hydrophobic C_{18} block and a hydrophilic PEG block. For PEGylated block copolymers, we detect well-defined micellar structures at low temperatures. Upon heating the system close to the LCST of PNIPAAM, we observe a two-step process: first the micelles collapse into smaller micelles at moderate temperature, followed by inter-micellar aggregation and finally macroscopic phase separation. Interestingly, the PEG content can effectively vary the thermoresponsive structure and the phase stability of the system. The micellar structure of the micelles has been analyzed using a detailed theoretical modeling analysis of the SAXS/SANS data. This analysis reveals a rather classical core–shell structure, at least at moderate temperatures. At higher temperatures, a significant shrinkage of the micelles is observed that can be attributed to the collapse of PNIPAAM chains. Interestingly, the analysis does not provide any evidence of back folding where PNIPAAM forms part of the core upon crossing the LCST.

This might be caused by prohibiting entropic penalty associated with the folding of polymer chains and/or enthalpic incompatibility between the blocks. The synthetic strategy and structural insight provided in this study might be of value for design of new thermoresponsive block copolymer systems for potential applications, such as in nanomedicine. In this respect, the system presented in this work constitutes a useful platform for the facile design of novel thermo-responsive nanostructures in the future.

Acknowledgements

The EMBL, Hamburg is gratefully acknowledged for allocation of the beamtime at the bioSAXS P12 instrument, Petra III. We are indebted to Dr Petr. Konarev for kind help and assistance during the SAXS experiments. Z.Q. acknowledges a scholarship from the Norwegian Research Council under the Cultural Agreement between Norway and China with the number 214658 and the Fundamental Research Funds for the Central Universities in China with the no. JB-ZR1117. B.N. and R.L. greatly acknowledge a grant from the Norwegian Research Council, SYNKNØYT, for the project with the number 8411/F50.

References

1 M. Irie, *Adv. Polym. Sci.*, 1993, **110**, 49.
2 M. A. C. Stuart, W. T. S. Huck, J. Genzer, M. Müller, C. Ober, M. Stamm, G. B. Sukhorukov, I. Szleifer, V. V. Tsukruk, M. Urban, F. Winnik, S. Zauscher, I. Luzinov and S. Minko, *Nat. Mater.*, 2011, **9**, 101.
3 Y. Wang, H. Xu and X. Zhang, *Adv. Mater.*, 2009, **21**, 2849.
4 A. K. Bajpai, S. K. Shukla, S. Bhanu and S. Kankane, *Prog. Polym. Sci.*, 2008, **35**, 1088.
5 S. Lin and P. Theato, *Macromol. Rapid Commun.*, 2013, **34**(14), 1118.
6 P. M. Mendes, *Chem. Soc. Rev.*, 2008, **37**, 2512.
7 S. Fujishige, K. Kubota and I. Ando, *J. Phys. Chem.*, 1989, **93**, 3311.
8 H. G. Schild, *Prog. Polym. Sci.*, 1992, **17**, 163.
9 K. Kubota, S. Fujishige and I. Ando, *J. Phys. Chem.*, 1990, **94**, 5154.
10 Y. Zhang, S. Furyk, L. B. Sagle, Y. Cho, D. E. Bergbreiter and P. S. Cremer, *J. Phys. Chem. C*, 2007, **111**, 8916.
11 Y. Xia, X. Yin, N. A. D. Burke and H. D. H. Stöver, *Macromolecules*, 2005, **38**, 5937.
12 R. Pamies, K. Zhu, A.-L. Kjøniksen and B. Nyström, *Polym. Bull.*, 2009, **62**, 487.
13 R. Lund and B. Nyström, 2013, in preparation.
14 M. Topp, P. J. Dijkstra, H. Talsma and J. Feijen, *Macromolecules*, 1997, **30**, 8518.
15 W. Zhang, L. Shi, K. Wu and Y. An, *Macromolecules*, 2005, **38**, 5743.
16 S. Qin, Y. Geng, D. E. Discher and S. Yang, *Adv. Mater.*, 2006, **18**, 2905.
17 J. E. Chung, M. Yokoyama, T. Aoyagi, Y. Sakurai and T. Okano, *J. Controlled Release*, 1998, **53**, 119.
18 R. C. W. Liu, S. Cantin, F. Perrot and F. M. Winnik, *Polym. Adv. Technol.*, 2006, **17**, 798.
19 P. Kujawa, H. Watanabe, F. Tanaka and F. M. Winnik, *Eur. Phys. J. E: Soft Matter Biol. Phys.*, 2005, **17**, 129.
20 P. Kujawa, F. Segui, S. Shaban, C. Diab, Y. Okada, F. Tanaka and F. M. Winnik, *Macromolecules*, 2006, **39**, 341.
21 T. Koga, F. Tanaka, R. Motokawa, S. Koizumi and F. M. Winnik, *Macromolecules*, 2008, **41**, 9413.
22 J. Adelsberger, A. Kulkarni, A. Jain, W. Wang, A. M. Bivigou-Koumba, P. Busch, V. Pipich, O. Holderer, T. Hellweg, A. Laschewsky, P. Müller-Buschbaum and C. M. Papadakis, *Macromolecules*, 2010, **43**, 2490.
23 J. Adelsberger, E. Metwalli, A. Diethert, I. Grillo, A. M. Bivigou-Koumba, A. Laschewsky, P. Müller-Buschbaum and C. M. Papadakis, *Macromol. Rapid Commun.*, 2012, **33**, 254.
24 C. Zhou, M. A. Hillmyer and T. P. Lodge, *J. Am. Chem. Soc.*, 2012, **134**, 10365.
25 C. Zhou, M. A. Hillmyer and T. P. Lodge, *Macromolecules*, 2011, **44**, 1635.
26 I. Koonar, C. Zhou, M. A. Hillmyer, T. P. Lodge and R. A. Siegel, *Langmuir*, 2012, **28**, 17785.
27 R. Narain and S. P. Armes, *Macromolecules*, 2003, **36**, 4675.
28 C.-G. Mu, X.-D. Fan, W. Tian, Y. Bai, Z. Yang, W.-W. Fan and H. Chen, *Polym. Chem.*, 2012, **3**, 3330.
29 M. Ciampolini and N. Nardi, *Inorg. Chem.*, 1966, **5**, 1150.
30 S. Liu and S. P. Armes, *J. Am. Chem. Soc.*, 2001, **123**, 9910.
31 N. Beheshti, K. Zhu, A.-L. Kjøniksen, K. D. Knudsen and B. Nyström, *Soft Matter*, 2011, **7**, 8111.
32 W. Wang, H. Mauroy, K. Zhu, K. D. Knudsen, A.-L. Kjøniksen, B. Nyström and S. A. Sande, *Soft Matter*, 2012, **8**, 11514.
33 K. Zhu, H. Jin, A.-L. Kjøniksen and B. Nyström, *J. Phys. Chem. B*, 2007, **111**, 10862.
34 K. Zhu, R. Pamies, A.-L. Kjøniksen and B. Nyström, *Langmuir*, 2008, **24**, 14227.
35 A.-L. Kjøniksen, A. Laukkanen, C. Galant, K. D. Knudsen, H. Tenhu and B. Nyström, *Macromolecules*, 2005, **38**, 948.
36 C. Sommer, J. S. Pedersen and P. C. Stein, *J. Phys. Chem. B*, 2004, **108**, 6242.
37 G. Beaucage, *J. Appl. Crystallogr.*, 1996, **29**, 134.
38 J. S. Pedersen, C. Svaneborg, K. Almdal, I. W. Hamley and R. N. Young, *Macromolecules*, 2003, **36**, 416.
39 J. Pedersen, *Small-Angle Scattering from Surfactants and Block Copolymer Micelles*, Springer, Berlin Heidelberg, 2008.
40 R. Lund, V. Pipich, L. Willner, A. Radulescu, J. Colmenero and D. Richter, *Soft Matter*, 2011, **7**, 1491.
41 R. Lund, L. Willner, V. Pipich, I. Grillo, P. Lindner, J. Colmenero and D. Richter, *Macromolecules*, 2011, **44**, 6145.
42 J. K. Percus and G. J. Yevick, *Phys. Rev.*, 1958, **110**, 1.
43 R. J. Baxter, *J. Chem. Phys.*, 1968, **49**, 2770.
44 J. Teixeira, *J. Appl. Crystallogr.*, 1988, **21**, 781.
45 M. Daoud and J. P. Cotton, *J. Phys.*, 1982, **43**, 531.
46 A. Halperin, *Macromolecules*, 1987, **20**, 2943.

47 J. S. Pedersen, D. Posselt and K. Mortensen, *J. Appl. Crystallogr.*, 1990, **23**, 321.
48 A. Malliaris, J. Le Moigne, J. Sturm and R. Zana, *J. Phys. Chem.*, 1985, **89**, 2709.
49 C. Sommer and J. S. Pedersen, *Macromolecules*, 2004, **37**, 1682.
50 S. Borbély, *Langmuir*, 2000, **16**, 5540.
51 G. Karlström, *J. Phys. Chem.*, 1985, **89**, 4962.